JOURNAL OF MATERIALS SCIENCE 3 (1968) 360–371

An Introduction to High-Voltage Electron Microscopy

M. J. MAKIN, J. V. SHARP
Metallurgy Division, United Kingdom Atomic Energy Authority Research Group, Atomic Energy Research Establishment, Harwell, Berks, UK

Received 19 February 1968

The various features of high voltage electron microscopy are examined in some detail, including basic features of the instrument such as lens aberrations, etc and more particularly, the effect of the microscope voltage on the behaviour of crystalline specimens, both in respect of the formation of diffraction contrast from defects and the production of radiation damage.

High accelerating voltages (i.e. 500 to 1000 kV) enable thicker foils (1 to 2 μm of medium atomic number materials and 4 to 8 μm of aluminium) to be used so that the foil behaviour is more typical of bulk material. In addition, diffraction patterns can be obtained from smaller precipitates and sharp dark field micrographs can be produced without beam tilting.

The major disadvantage is probably the formation of radiation damage by displacement of atoms when the electron energy exceeds a threshold value.

1. Introduction

The ability of the electron microscope to reveal the microstructure (including dislocations and defect clusters) with a resolution of 20 Å or less in a thin specimen has resulted in great progress in many fields in the past ten years. Inevitably however, the technique has had its limitations, and the most serious of these is the thinness of the specimens required (at 100 kV $\sim$ 500 — 5000 Å depending on material). It has been shown that in many circumstances the behaviour of such specimens is dominated by the close proximity of the surfaces and is not typical of bulk material.

The most practicable way of increasing the penetration is by increasing the energy of the electron beam, and now that methods of stabilising high voltage supplies of up to 1 MV have been devised, such microscopes are becoming commercially available. In addition to the increased penetration there are many other features in which high voltage microscopes differ from 100 kV instruments, and these are explored in this paper.

2. General Design

The same basic electron optical system is used of electron source, accelerator, double condenser lens, objective and projector lenses, followed by viewing screen and camera. At 100 kV an integral gun and accelerator is used in which electrons are emitted from an area of a hot filament and accelerated by the potential between the filament and the anode plate. The theoretical brightness β obtainable is given by the Langmuir formula

$$\beta = \frac{\rho_c E}{\pi kT}$$

where ρ_c is the current density in the filament, E is the accelerating voltage, k is Boltzmann's constant, and T the temperature. Hence the brightness is a linear function of the accelerating voltage.

In high voltage microscopes a normal gun is used to produce a beam of low energy electrons (typically 5 to 50 keV) which then pass down a tube in which they are accelerated in stages to the energy required. The high voltage is gener-

ated by a Cockcroft-Walton circuit and the equipment can be either air or gas (SF_6 or Freon) insulated. The latter provides a much more compact installation and being in a sealed tank (or tanks) less stringent control of the environment is required.

As in 100 kV microscopes, electromagnetic lenses with soft iron pole pieces are used for all present high voltage microscopes. The size of the lenses increases rapidly with voltage however, since as the field strength possible with soft iron pole pieces is limited, the path lengths in the lenses must be increased. Much larger coils and yokes are consequently required. A useful consequence of the larger path lengths in the lenses is an increase in the volume available around the specimen for auxiliary stage equipment. Substantial X-ray shielding is required (6 to 10 in.* of iron at 1 MV) and hence the column is of considerably greater dimensions than is required at 100 kV. At 1 MV a typical column would be 5 to 6 ft high and 15 to 18 in. in diameter. The column height is also increased by the need to include a third projector lens. The purpose of this is to enable the camera length to be increased by an order of magnitude so that the diffraction spots are more widely spaced. The spacing x ($x = \lambda L/d$ where L is the camera length, λ the wavelength of the electron beam, and d the interplanar spacing) is only a millimetre or so at high voltages unless L is substantially increased from its typical value at 100 kV of about 40 cm.

3. Diffraction Contrast

In transmission electron microscopy the normal method of image formation is by diffraction contrast, e.g. an aperture is placed near to the back focal plane of the objective lens so that it intercepts all the diffracted rays. In crystalline materials diffracted, or scattered, rays are formed by both *elastic* and *inelastic* scattering.

3.1. Elastic Scattering

In this the electron is scattered by effectively the whole atom and hence, because of the disparity in masses, there is only a negligible energy loss. In crystals elastic scattering is coherent in specific directions and Bragg reflections occur. Elastic scattering does not impose any limit on the thickness of crystal which can be penetrated, since repeated Bragg reflections can occur between the incident and diffracted beams. As the thickness of the specimen increases the intensity in each beam oscillates between zero and the full intensity, the two intensities being exactly out of phase. The cross section for elastic scattering is measured by the "extinction distance" ξ_g which is the wavelength of this intensity oscillation when the lattice planes are exactly at the Bragg angle.

*1.0 in. = 2.5 cm.

TABLE I Electron parameters.

kV	λ (Å)	v/c	m/m_0	v/v_{100}
100	0.0370	0.548	1.196	1.000
200	0.0251	0.695	1.391	1.268
300	0.0197	0.777	1.587	1.416
400	0.0164	0.828	1.783	1.510
500	0.0142	0.863	1.979	1.574
600	0.0126	0.888	2.174	1.620
700	0.0113	0.907	2.370	1.654
800	0.0103	0.921	2.566	1.680
900	0.0094	0.932	2.761	1.700
1000	0.0087	0.941	2.957	1.717

The change in Bragg angles and extinction distances with voltage can readily be calculated from the variation in the electron parameters with energy (table I). The electron wavelength λ decreases rapidly with voltage since $\lambda = h/mv$, where h is Planck's constant, and m and v are the mass and velocity of the electron, and hence there are corresponding decreases in the Bragg angles θ, since $n\lambda = 2d \sin \theta$ where d is the interplanar spacing ($\theta_{1\,MV} \simeq 0.23\theta_{100kV}$). Extinction distances for two beam diffraction conditions can be calculated from table I by the relation

$$\xi_g(E) = \frac{v}{v_{100}} \xi_g(100\,\text{kV}) \qquad (1)$$

This relation is derived from the expression $\xi_g = 1/\lambda U_g$ where $U_g = V_g\,(2me/h^2$ (where V_g is the Fourier coefficient of the crystal lattice potential which is, of course, independent of voltage.

The occurrence of Bragg reflections can be determined by the intersection of the Ewald sphere with the reciprocal lattice of the crystal (fig. 1). A Bragg reflection is excited only when the reciprocal lattice point lies within a distance of $\sim 1/2\xi_g$ of the sphere. Since ξ_g increases with voltage (equation 1), Bragg reflections occur over a smaller range of lattice orientations at high voltages.

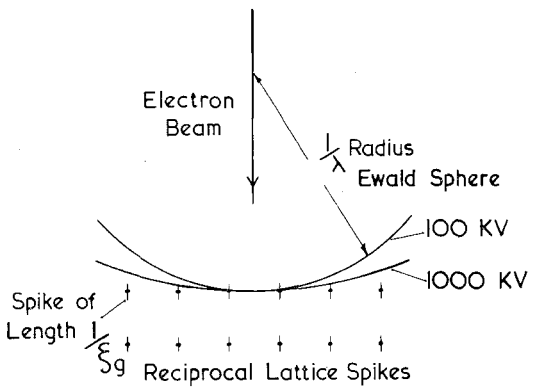

Figure 1 Construction of the Ewald sphere, showing why multiple beam conditions occur more readily at high voltages.

The radius of the Ewald sphere is $1/\lambda$ and hence is much larger at high voltages. Since λ changes more rapidly with voltage than ξ_g the number of reflections excited of the type ng, where the g reflection is fully excited, is increased. These are known as the "systematic reflections" and when they are present "multiple beam conditions" are said to exist. These occur more frequently in materials of high atomic number since $1/\xi_g$ is greater in these materials.

3.2. Inelastic Scattering

Inelastic scattering, which results from collisions with atomic electrons, produces an energy loss. There are several different inelastic scattering processes, including ionisation, excitation and plasmon scattering. Plasmon scattering takes place mainly through sharply defined "characteristic" energy losses of between a few eV and $\sim$ 100 eV. These arise by interactions between the bombarding electron and the plasma of electrons in the crystal. The plasma possesses characteristic frequencies of vibration and the discrete losses are each the result of the emission of a plasma oscillation quantum or "plasmon". The scattering is strongly peaked in the forward direction (i.e. confined to angles of $\sim 1/100 \times$ Bragg angle). The mean free path λ_p for plasmon excitation is of the order of 1000 Å at 100 kV and hence in a thick specimen several plasmons may be excited per electron. There is little information on how λ_p varies with voltage.

In crystals, inelastic scattering produces three deleterious effects on the image. Firstly, electrons scattered through a large angle are stopped by the objective aperture so resulting in a decrease in intensity. Secondly, inelastic collisions tend to destroy the coherence of the beam so producing wider images of lower contrast, and thirdly, inelastic scattering produces chromatic aberration and hence a loss of resolution. The maximum thickness of usable foils is in fact limited by the effects of inelastic scattering.

A phenomenological treatment of "absorption" has been given by Hashimoto, Howie and Whelan [1], who modified the dynamical theory by introducing an imaginary addition $iV'(r)$ to the crystal potential $V(r)$. The effect of this is to introduce an attenuation term $e^{-\mu t}$ where t is the thickness and $\mu = 2\pi/\xi_0'$ for the straight through beam and $2\pi[(1/\xi_0') - (1/\xi_g')]$ for the g^{th} diffracted beam. ξ_0' and ξ_g' are given by exactly equivalent expressions to ξ_0 and ξ_g i.e.

$$\xi_0' \propto \frac{v}{V_0'} \text{ and } \xi_g' \propto \frac{v}{V_g'}$$

From the theory of inelastic scattering [2] V_0' and V_g' are inversely proportional to v so that ξ_0', $\xi_g' \propto v^2$ and hence μ_0, $\mu \propto 1/v^2$. This decrease in inelastic scattering cross section is the reason for the increase in penetration with voltage. The theory predicts that thickness $t \propto v^2$.

The effect of systematic reflections, or multiple beam conditions, on the absorption coefficient has recently been calculated in fcc crystals in the (111) reflecting position by Howie [3] and Humphreys [4]. Howie used ten beams and calculated the current distribution in the four most strongly excited Bloch waves. The results for copper, fig. 2, show that wave 3 channels increasingly well at higher voltages whereas wave 1 channels less well. In fig. 2 the absorption coefficients for waves 1 and 3 are plotted as a function of voltage for copper, aluminium and gold. The v^2 term has been extracted so that $t \propto v^2$ would give a constant value of μ. It can be seen that up to a critical voltage $\mu_{(1)}$ increases with voltage so that the penetration will increase less rapidly than $t \propto v^2$. Above the critical voltage $\mu_{(3)}$ becomes less than $\mu_{(1)}$ and decreases with increasing voltage, so that the penetration will increase more rapidly than $t \propto v^2$. The critical voltage is expected to be lowest in the heavy elements and is 180 kV in gold, 650 kV in copper and 1500 kV in aluminium. In gold Howie predicts that for a given attenuation factor (I/I_0) $t_{1MV}/t_{100kV} \simeq 12$.

Humphreys [4] has calculated that in copper crystals in the (111) reflecting position there is a factor of two increase in penetration between

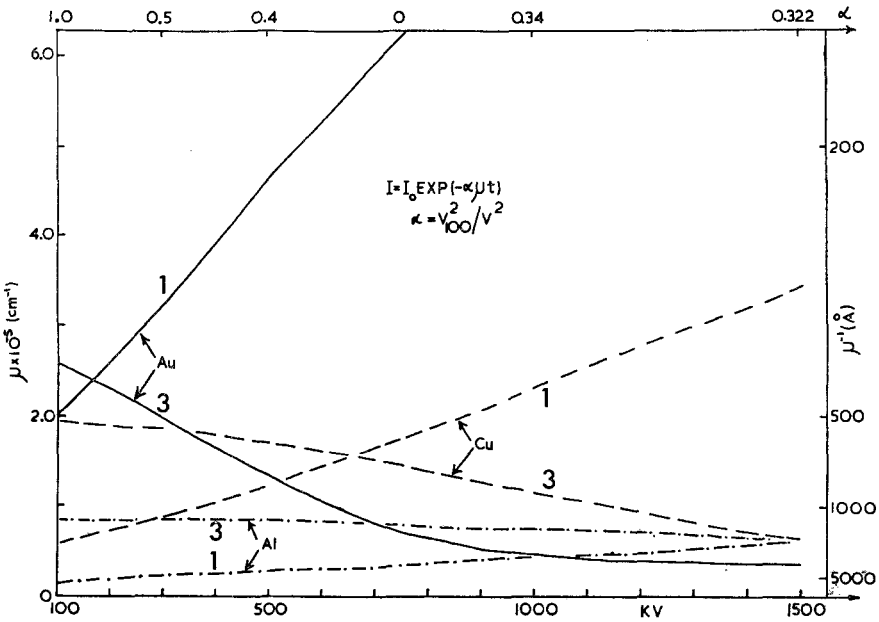

Figure 2 Accelerating voltage dependence of the intensity attenuation coefficient μ for Bloch waves 1 and 3 for A Cu, and Au at the (111) Bragg reflecting position. The v^2 dependence has been extracted in the factor $\alpha = v^2_{100}/v^2$ [$I = I_0 \exp(-\alpha\mu t)$] where t is the thickness. Values of α are shown along the top of the diagram. The attenuation coefficient for wave 1 increases with increasing voltage whereas that for wave 3 decreases (after Howie [3]).

100 and 500 kV, little change between 500 and 1000 kV and a further 50% increase between 1000 and 2000 kV.

4. Lens Aberrations

4.1. Spherical Aberration

The ultimate resolution of an electron microscope is limited by spherical aberration (a failure to focus rays parallel to the axis but displaced from it in the same plane as axial rays) in the objective lens. The radius of the circle of least confusion r_s is given by $r_s \simeq C_s\alpha^3$ where C_s is the spherical aberration coefficient of the lens ($\approx$ focal length) and α is the effective aperture semi-angle*. Hence although spherical aberration can be made small by reducing α there is another effect, the formation of diffraction fringes around an image, which limits the resolution to $0.61\lambda/\alpha$. There is therefore an optimum aperture given by $\alpha = (0.61\lambda/C_s)^{\frac{1}{4}}$. At the optimum aperture the resolution is hence $\delta \approx 0.7\ (C_s\lambda^3)^{\frac{1}{4}}$. The variation of $(C_s\lambda^3)^{\frac{1}{4}}$ (and hence resolution) with voltage for a typical lens has been calculated by Cosslett [5] and is shown in fig. 3. The improvement in the theoretical resolution with increasing voltage is rapid up to 500 kV.

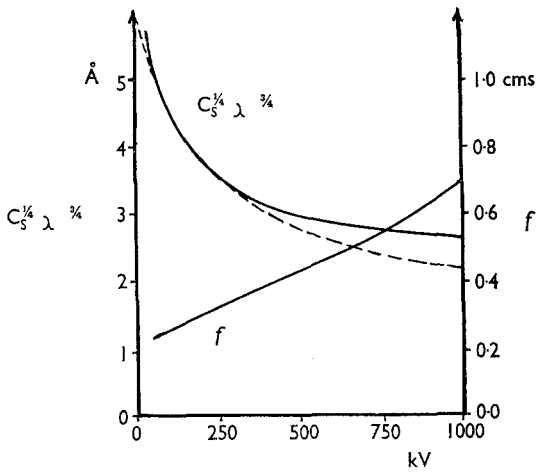

Figure 3 Variation of the parameter $C_s^{\frac{1}{4}}\ \lambda^{\frac{3}{4}}$ and objective focal length f with accelerating voltage, where C_s is the spherical aberration coefficient and λ the electron wavelength. The dotted curve shows the variation in $(C_s\ \lambda^3)^{\frac{1}{4}}$ when the lens dimensions are increased with voltage (after Cosslett [5]).

There are two practical consequences of the reduced Bragg angle and hence spherical

*Note that α may be less than the value given by the objective aperture stop if the cone of rays lies within the stop.

aberration at high voltages; increased accuracy of selected area diffraction and sharper dark field micrographs.

TABLE II Accuracy of selected area diffraction.

Reflection (aluminium)	100 kV*		1000 kV†	
	α	$C_s\alpha^3$ (Å)	α	$C_s\alpha^3$ (Å)
111	1.58×10^{-2}	130	3.73×10^{-3}	2.6
222	3.16×10^{-2}	1050	7.46×10^{-3}	21
333	4.74×10^{-2}	3540	11.2×10^{-3}	70

*C_s (100 kV) = 3.3 mm (Elmiskop)
†C_s (1000 kV) = 5 mm (A E I Microscope)

In a diffraction pattern the direct and diffracted beams originate from different areas of the specimen separated by a distance of $\sim 8C_s\theta^3$ where θ is the Bragg angle. The selector aperture is placed in the image plane of the objective lens, and due to spherical aberration, the position of the "image" of this aperture in the specimen plane depends on the direction of the rays emitted from the specimen. Since the Bragg angle θ is $\lambda/2d$ the value of $8C_s\theta^3$ is greatly reduced at high voltages (table II) and this has been experimentally demonstrated by Dupouy *et al* [6]. The small errors involved for low order reflections at high voltages make it possible to obtain diffraction patterns from very small precipitates. In interpreting such patterns it should be remembered that higher order spots are increasingly likely to originate from the matrix. Note that through incorrect focusing the image of the selector aperture may not accurately coincide with the specimen, introducing a further error of $\sim 2D\theta$, where D is the distance between the specimen and the conjugate image of the aperture. At 100 kV, D can be as large as 10 μm for a thick specimen resulting in an error of 1600 Å for the (111) reflection in aluminium. At 1 MV the corresponding error is 370 Å. Hence in practice the error due to incorrect focusing may easily be dominant.

It is obvious that the reduced Bragg angles and consequently smaller spherical aberration at high voltages will result in sharper dark field micrographs. It has been observed that to obtain good resolution for low order spots it is unnecessary to tilt the incident beam such that the emergent beam lies on the optic axis, as has to be done at 100 kV.

4.2. Chromatic Aberration

In electron optics chromatic aberration is the loss of resolution due to the failure of the lens to bring electrons of differing energies to focus in the same plane, i.e. to a variation in the focal length with energy. It arises both from the instrument (variations in accelerating voltage or lens current supplies) and from energy losses by inelastic scattering in the specimen. The resolution r_c is given by

$$r_c \simeq C_c\,\alpha(\Delta E/E) \qquad (2)$$

where C_c is the chromatic aberration constant of the lens and α is the *effective* semi-angle of the beam at the objective aperture, E is the accelerating voltage. The product $C_c\alpha$ is to a first approximation independent of voltage and hence for a given ΔE the resolution is proportional to $1/E$.

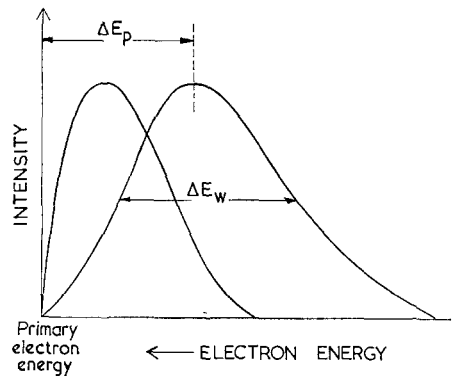

Figure 4 Energy distribution of electrons after passing through a specimen. The terms ΔE_p and ΔE_w are defined. The electron beam is initially monoenergetic; it can be seen that both ΔE_p and ΔE_w increase with increasing specimen thickness.

An initially monoenergetic beam passing through a solid (i) acquires a distribution of energies of finite width and (ii) decreases in mean energy, as a result of inelastic collisions. This is illustrated in fig. 4, where the terms ΔE_p and ΔE_w are defined. Chromatic aberration arises only from ΔE_w, and if this is known the loss of resolution can be calculated from equation 2. Values of ΔE_p and ΔE_w for amorphous materials have been predicted by Landau [7]

$$\Delta E_p = W_1\,\{\ln[mv^2W_1/I^2(1-\beta^2)] - \beta^2 - 0.37\}$$

where $W_1 = 2\pi e^4NZt/mv^2$ and $\Delta E_w = 3.98\ W_1$;

I is the ionisation energy, e the electronic charge (in esu), N the number of atoms per cm^3, Z the atomic number, t the specimen thickness, m the electron rest mass and v the electron velocity, $\beta = v/c$ where c is the velocity of light. Values of $(\Delta E_p)_{theor}$ and $(\Delta E_w)_{theor}$ for Al and Cu are given in table III.

The experimental determinations of ΔE_w and ΔE_p in MgO crystals at 500 kV by Kamiya [8] have been compared with values calculated from the Landau expression. The measured values of ΔE_w are greater than $(\Delta E_w)_{theor}$ by a factor of ~ 2, but are approximately given by the relation $(\Delta E_w)_{exp} \simeq (\Delta E_p)_{theor}$ The decrease with voltage, in $(\Delta E_p)_{theor}$ given in table III when substituted in equation 2, shows that for a constant thickness the resolution due to chromatic aberration improves by a factor of over twenty between 100 kV and 1 MV. Similarly, for a constant resolution the increase in thickness is nearly linear with voltage (curve A in fig. 5) and increases by an order of magnitude between 100 kV and 1 MV.

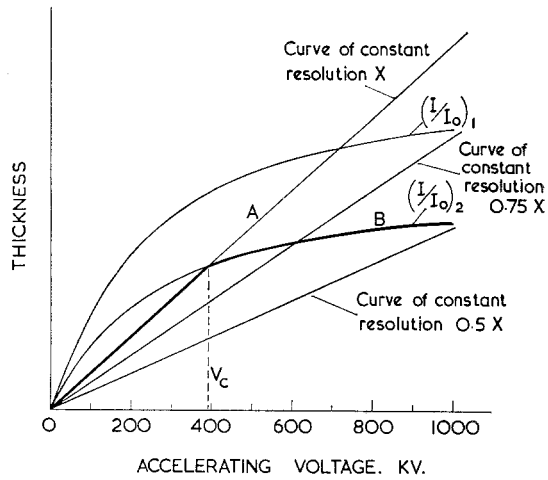

Figure 5 Schematic diagram of the criteria which limit the usable foil thickness. For the two curves selected A and B there is a critical voltage V_c below which resolution is limiting and above which intensity is limiting. Although the usable specimen thickness increases only slowly above V_c there is a significant gain in resolution at higher voltages.

5. The Increase in Usable Foil Thickness with Voltage

5.1. General Considerations

The decrease in inelastic scattering cross section and consequent increase in the thickness of usable foils is the principal reason for the adoption of high voltages for microscopy. Theoretically the situation is complex however, since at present the nature of the factor limiting the maximum usable thickness in practice is not clearly understood. As explained previously there are three possibilities, loss of intensity, loss of resolution due to chromatic aberration and loss of contrast and resolution through incoherence.

The intensity I reaching the screen is related to the incident intensity I_0 by the relation

$$I = I_0 e^{-\mu t}$$

On the simple theory (i.e. neglecting multiple beams) $\mu \propto 1/v^2$ and hence $t \propto v^2$ for a constant I/I_0. Curves of this type are shown in fig. 6. Hence to obtain the maximum possible penetration it is important to be able to work with very low values of I/I_0. The minimum value depends on the necessity of focusing the image on the

TABLE III Maximum probable energy ΔE_p and half-width ΔE_w calculated from the Landau expression.

Voltage (kV)	Thickness (μm)	Al		Thickness (μm)	Cu	
		ΔE_p (eV)	ΔE_w (eV)		ΔE_p (eV)	ΔE_w (eV)
100	0.1	33	27	0.1	102	83
	0.5	218	133	0.5	677	417
	1.0	482	265	1.0	1498	833
	4.0	2295	1060	1.5	2375	1250
500	0.1	15	11	0.1	46	34
	0.5	95	54	0.5	297	168
	1.0	210	107	1.0	652	336
	4.0	987	428	1.5	1030	504
1000	0.1	14	9	0.1	43	28
	0.5	88	45	0.5	273	141
	1.0	191	90	1.0	595	282
	4.0	890	360	1.5	936	423

screen and hence on the beam current and the efficiency of the screen. The use of an image intensifier should clearly be advantageous for focusing purposes.

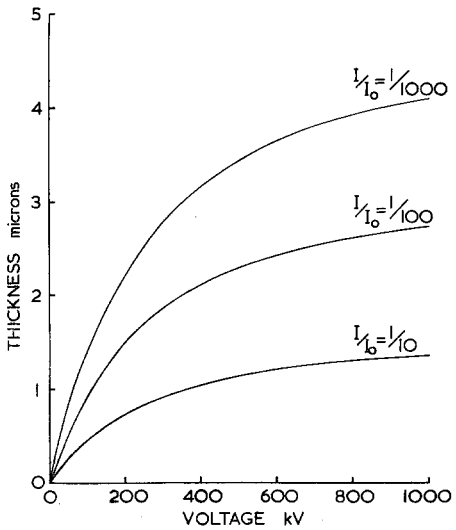

Figure 6 The relation between specimen thickness and accelerating voltage in Al for three different values of I/I_0 where I_0 is the initial electron beam intensity and I is the beam intensity after passing through the specimen. The curves have been calculated for an absorption coefficient μ, of 2×10^4 cm^{-1} at 500 kV. This value gives results in reasonable agreement with experiment.

If we assume that a sufficiently low value of I/I_0 can be used then a further possible limit may be the loss of resolution due to chromatic aberration. As shown previously, this gives rise to a family of nearly linear relationships (curve A in fig. 5) between thickness and voltage for different values of the resolution required. Clearly these can be superimposed on the curves in fig. 6, and this has been done in fig. 5. When both resolution and intensity (or contrast) can be limiting (e.g. curves A and B in fig. 5) the variation in thickness with voltage can be divided into regions above and below V_c, the voltage at which the curves intersect. Below V_c resolution is limiting and above V_c intensity is limiting. Unfortunately the relative position of the two sets of curves has not yet been established in any existing microscope. A somewhat similar but different analysis is contained in a recent publication by Cosslett [9].

Little is known about the effect of incoherence on the resolution and contrast of images of defects. In traversing a thick specimen almost all the electrons lose energy by inelastic scattering and hence the incident coherent beam becomes spread in both energy and direction and hence loses its coherence. For small energy losses and angular deviations it appears that some coherence is retained since these electrons form images which are similar to those formed by elastically scattered electrons (Kamiya and Uyeda [10]). Images for different energy losses do not necessarily coincide exactly with each other so that there is in general some loss of resolution. As the energy loss increases the coherence is gradually lost and the scattered electrons contribute largely to the background intensity on the screen so that the *contrast* is reduced. Since this loss of contrast is due to inelastic scattering it is reasonable to assume that it will give a $t \propto v^2$ dependence of thickness on electron energy. This is the same dependence as the loss of intensity, and hence the curves in fig. 5 can refer qualitatively either to loss of intensity or loss of contrast.

5.2. Experimental Measurements

Measurements have been made as a function of voltage of both the absorption coefficient μ and the foil thicknesses in which dislocation images are resolvable.

The absorption coefficient is obtained by measuring the profiles of thickness fringes in a wedge shaped specimen. The absorption coefficient is given by $\mu = 1/\xi_g \ln [(I_n)/(I_{n+1})]$ where I_n is the intensity of the n^{th} fringe. These measurements have been made for aluminium over the range 100 to 300 kV (Hashimoto *et al* [11]), MgO between 100 to 1200 kV (Dupouy *et al* [12]) and aluminium and stainless steel between 100 to 500 kV (Fujita *et al* [13]). In the lower voltage experiments on the metals it was found that $\mu \propto 1/v^2$ as predicted by the simple theory of inelastic scattering. In MgO, however, deviations were found at high voltages which are claimed by Goringe *et al* [14] to be consistent with multiple beam effects. Note that thickness fringe measurements do not provide a reliable guide to the foil thickness in which defects are visible since fringes are only observed when there is an appreciable intensity in more than one Bloch wave.

Measurements of the usable foil thickness in which defects can be observed have been made for a number of materials. Unfortunately these have to date been only semi-quantitative

investigations in that the contrast and resolution have been estimated rather than measured.

Studies of the thickness/voltage curve have been made by Uyeda [15] (MoS_2), Hale [16] (iron), Sharp and Poole [17] (copper and UC), Dupouy and Perrier [18] (aluminium), and Fujita *et al* [13] (aluminium, iron and copper). The dependence of the results on the conditions under which they were taken is reflected in the values obtained, which at 500 kV are 4 to 8 μm in aluminium, 0.8 to 2.0 μm in copper, 1.0 to 2.0 μm in iron. Most authors report that resolution is not limiting, but that the higher figures are obtained only by prolonged exposures of very faint images, the lower figures refer to normal, i.e. fairly bright screen, conditions. Furthermore, Hale, Sharp and Poole, and Dupouy *et al* report a further substantial increase in penetration (i.e. 30 to 50%) between 500 and 800 to 1000 kV. This is in marked contrast to the $t \propto v^2$ result, where the increase is $\sim 20\%$.

The more detailed work of Uyeda on MoS_2, however, does not agree with the above measurements and shows a $t \propto v^2$ dependence, the penetration at 500 kV being 4 to 5 μm. Uyeda concludes that the ultimate limit in penetration is imposed by lack of contrast, although to work to this limit involves taking photographs when the intensity of the fluorescent screen is very low. Uyeda found that this limit occurs when the diffraction pattern contains Kikuchi lines and two residual spots. Thicker specimens, which show only Kikuchi patterns, do not yield resolvable images.

There need be no contradiction between the two sets of results however, if it is assumed that resolution was the important criterion in the results on the metals. If this were so then a nearly linear relationship would be expected from the chromatic aberration relationship.

6. Radiation Damage in the Specimen

6.1. Ionisation

Energy loss by ionisation is dominant for energies below 1 MeV and the rate of energy loss calculated from the formula given by Bethe [19] is shown in fig. 7. In conducting materials, such as metals, ionisation is only a transient phenomenon and produces no observable effects. In insulating crystals, however, serious effects can occur such as colour centre production in ionics, crosslinking and degradation in polymers, etc. The study of these materials by electron microscopy is very restricted for this reason and hence the factor of two reduction between 100 and 500 kV is an advantage, although image intensification offers much greater potential reductions.

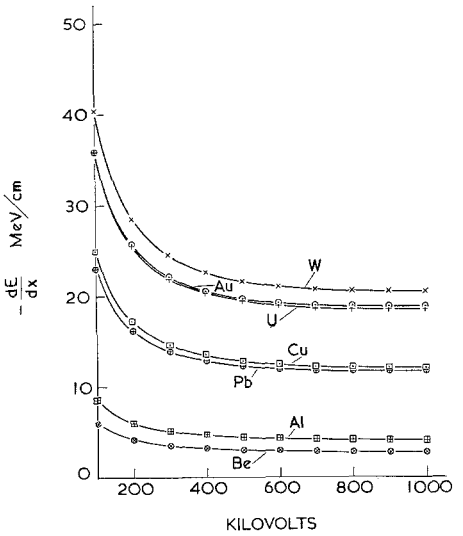

Figure 7 Energy loss per unit specimen thickness ($-dE/dx$) in MeV/cm or eV per 100 Å as a function of accelerating voltage, for a range of materials. The value of $-dE/dx$ is calculated from the Bethe formula.

The reduction in ionisation at high voltages reduces the brightness per unit thickness of screen. This can be overcome with a thicker screen since the total energy available is much greater, but only at the cost of decreased resolution due to electron scattering. Also, absorption of light in the phosphor decreases the gain in brightness achieved.

Similar considerations apply to photographic emulsions which are $\sim$ 100% efficient at 100 kV. The relative increase in exposure is $\sim$ 3 times between 100 kV and 1 MV. Different results are expected in plates and film, due to the greater backscatter in the former, and this will also adversely affect the resolution.

Another consequence is the lower rate of specimen contamination at high voltages. This occurs by the decomposition of organic molecules absorbed on the specimen in dynamic equilibrium with the concentration in the microscope vacuum.

Experiments by Bahr, Zeitler, and Kobayashi [20] have demonstrated the reduction at high voltages. Contamination can, however, be removed effectively by cold plate devices which reduce the partial pressure of organic molecules in the specimen area.

6.2. Displaced Atoms

The maximum energy transferred between an electron and an atom is given by

$$E_m = \frac{2E(E + 2mc^2)}{M_2c^2}$$

where M_2 is the mass of the struck atom. The variation of E_m with E for copper is shown in table IV. When E_m exceeds the displacement energy, E_d, the struck atom is displaced, so creating an interstitial-vacancy pair. The values of E for which $E_m = E_d = 25$ eV are given in table V for a number of elements ($E_d \simeq 25$ eV is generally accepted as a reasonable average value). When $E_m > E_d$ the cross section for displacement σ_p is given by (Dugdale and Green [21])

$$\sigma_p = \frac{4Z_2^2E_R^2}{m^2c^4}\left(\frac{E_m}{E_d}\right)\pi a_0^2\left(\frac{1-\beta^2}{\beta^4}\right)\left\{1 + 2\pi\alpha\beta\left(\frac{E_d}{E_m}\right)^{\frac{1}{2}} - \left(\frac{E_d}{E_m}\right)\left[1 + 2\pi\alpha\beta + \left(\beta^2 + \pi\alpha\beta\right)\ln\left(\frac{E_m}{E_d}\right)\right]\right\}$$

where Z_2 is the atomic number of the specimen material, $E_R = 13.6$ eV and $\pi a_0^2 = 8.8 \times 10^{-17}$ cm^2 and $\alpha = Z_2/137$. Values of E_m and σ_p in copper are given in table IV together with values of the mean energy $\bar{E}$ of the primary knock-ons and the number N_d of displacements per primary knock-on. $\bar{E}$ is given by

$$\bar{E} = \frac{E_dE_m}{E_m - E_d}\ln\left(\frac{E_m}{E_d}\right)$$

and

$$N_d = \left(1 + \ln\frac{E_m}{2E_d}\right)$$

when $E_m > 2E_d$. The concentration of displacements per second, C, is given by $\sigma_p\phi N_d$ where ϕ is the electron flux and is also quoted in table IV for a flux of 5.0×10^{18} e/cm^2/sec; i.e. a beam current of 0.2 μA in a 5 μm spot (current density 0.8 A/cm^2). Note that these figures do not allow for the channelling of electrons which occurs in crystals oriented for anomalous transmission. This can reduce the figures quoted by a factor of up to about five, depending on the conditions. The defect production rates C are very high at high energies ($\sim$1000 times greater at 1 MV than in many radiation damage experiments using accelerators, each atom is being displaced on average once every 80 min). Fortunately $\sim$80 to 90% of the interstitial-vacancy pairs produced at <1 MeV are *close* pairs and at normal temperatures recombine with each other very rapidly. The defects produced have two potential effects, firstly they may combine to form defect clusters as are observed after heavy particle or neutron irradiation, and secondly they will increase the effective diffusion coefficient. No defect clusters have been observed to form in copper during electron irradiation at room temperature*. Recently however, cluster formation has been observed at low temperatures in both copper and gold [22].

TABLE IV Maximum energy transferred E_m, cross section σ_p, mean energy of primary knock-ons $\bar{E}$, number of displaced atoms per primary knock-on N_d and concentration of displacements per second, as a function of accelerating voltage in copper.

kV	E_m(eV)	σ_p(barn)	$\bar{E}$(eV)	N_d	Conc/sec
100	3.8	—	—	—	—
200	8.3	—	—	—	—
300	13.0	—	—	—	—
400	19.0	—	—	—	—
500	26.0	0.74	25.4	1.00	3.7×10^{-6}
600	33.0	7.90	28.6	1.00	4.0×10^{-5}
700	41.0	14.70	31.6	1.00	7.4×10^{-5}
800	49.0	21.00	34.4	1.00	1.1×10^{-4}
900	58.0	26.50	37.1	1.20	1.6×10^{-4}
1000	68.0	31.50	39.6	1.30	2.1×10^{-4}

TABLE V The value of the accelerating voltage E, at which the maximum energy transferred to an atom equals 25 eV.

Element	Atomic Weight M_2	E (kV)
C	12.0	130
Al	27.0	248
Si	28.1	257
Fe	55.8	444
Cu	63.6	494
Mo	96.0	664
Ag	107.9	723
Ta	180.9	1030
W	183.9	1042
Au	197.2	1092
U	238.1	1233

**Note added in proof* Recent experiments using the Cambridge 750 kV microscope have shown that defect clusters can be produced in copper during room temperature observation (M. J. MAKIN, in press)

The increase in diffusion coefficient under steady state conditions can be readily estimated from formulae given by Lomer [23] and Dienes and Damask [24]. The diffusion coefficient during irradiation D_{irr} is given by

$$D_{irr} = v\nu_v\lambda^2 + i\nu_i\lambda^2$$

where v and i are the vacancy and interstitial concentrations, ν_v and ν_i are the vacancy and interstitial jump rates and λ is the jump distance. When defects are both recombining and diffusing to sinks $v\nu_v\lambda^2 = i\nu_i\lambda^2$ and $D_{irr} = 2v\nu_v\lambda^2$. The jump frequency

$$\nu_v = A_2 \exp -\left(\frac{E_m{}^v}{kT}\right)$$

where $A_2 = \nu \exp S_m{}^v/k = 10^{15}$ sec^{-1}, ν is the atomic frequency, and $S_m{}^v$ is the entropy of migration. $E_m{}^v$ is the activation energy of migration, ~ 0.8 eV in copper. The value of v is given by

$$v = -\tfrac{1}{2}(\alpha\lambda^2 + v_0) + \tfrac{1}{2}\left[(\alpha\lambda^2 + v_0)^2 + \frac{4K}{\nu_v}\right]^{\frac{1}{2}}$$

where K is the concentration of defects produced per second by the irradiation. In this expression α is a factor related to the density of fixed sinks, i.e. dislocations and the foil surfaces. For a dislocation density of N_0 in a foil of thickness L

$$\alpha = \frac{2\pi N_0}{\ln (r_1/r_0)} + \frac{\pi^2}{6L^2} \qquad \text{(see table VI)}$$

where $\pi_r{}^2 = 1/N_0$ and r_0 is the core radius of a dislocation ($\sim 3 \times 10^{-8}$ cm). The thermal vacancy concentration v_0 is given by

$$v_0 = \exp\left(\frac{S_f{}^v}{k}\right) \exp\left(\frac{-E_f{}^v}{kT}\right)$$

where the entropy factor $\exp (S_f{}^v/k) \approx 1$ and $E_f{}^v$ is the vacancy formation energy.

Steady state values of D_{irr} for copper are shown in fig. 8 as a function of α and specimen temperature for a beam current of 0.8 A/cm^2 of 1 MV electrons, assuming 90% direct recombination. For low values of α enhanced diffusion persists up to 800° K. The steady state effect is large at low temperatures, i.e. at 20° C the effective temperature is 600° K and the equilibrium concentration of vacancies is $\sim 5 \times 10^{-3}$. Since D_{irr} is proportional to $K^{\frac{1}{2}}$ when α and v_0 are small, the reduction in the effective temperature as the accelerating voltage is decreased is small until the threshold voltage is approached.

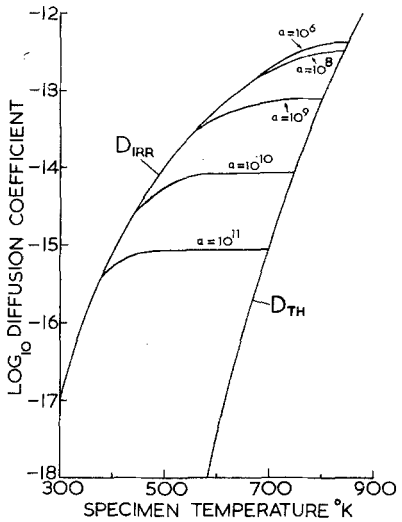

Figure 8 Values of the steady state diffusion coefficient D_{irr} (cm^2/sec) in copper due to electron irradiation, for various specimen temperatures and for different values of the sink density α.

The results given in fig. 8 must be applied with caution, since they refer only to steady state conditions, and the time required to reach these can be very long in some materials. For example

TABLE VI Values of α in foils of thickness L containing a dislocation density N_0/cm^2. Above the upper dotted line, α is controlled by the foil thickness and below the lower dotted line by the dislocation density.

N_0	Foil thickness L(Å)				
	1000	2000	3000	5000	10000
10^5	1.64×10^{10}	4.10×10^9	1.82×10^9	6.56×10^8	1.64×10^8
10^6	1.64×10^{10}	4.10×10^9	1.82×10^9	6.56×10^8	1.64×10^8
10^7	1.64×10^{10}	4.10×10^9	1.82×10^9	6.63×10^8	1.71×10^8
10^8	1.64×10^{10}	4.18×10^9	1.90×10^9	7.39×10^8	2.47×10^8
10^9	1.74×10^{10}	5.08×10^9	2.80×10^9	1.64×10^9	1.15×10^9
10^{10}	2.84×10^{10}	1.61×10^{10}	1.38×10^{10}	1.27×10^{10}	1.22×10^{10}
10^{11}	1.70×10^{11}	1.58×10^{11}	1.56×10^{11}	1.54×10^{11}	1.54×10^{11}

in annealed copper (i.e. low α) the irradiation time at 20° C required to build up half the final vacancy concentration is greater than 100 h. In general the time required to reach the steady state is decreased by increased α and by increased defect mobility, for example, when α is 10^{11} in copper at 20° C the corresponding time is less than 1 sec.

Enhanced diffusion should be considered in all experiments in which defects are produced during observation. Particular care is needed in experiments on unstable materials, such as solution-treated alloys, and also when quantitative measurements of parameters such as flow stress are being made in the microscope. The effects produced in alloys are not, of course, simply equivalent to an ageing treatment at the effective temperature. In general other parameters as well as the diffusion rate are important, for example the stability of small clusters must be considered, and this is unlikely to be affected by the electron irradiation.

Preliminary experiments on solution treated (and aged at 20° C for 1 day) Cu/Be and Al/Cu alloys showed no significant change in microstructure after 10 min observation at 600 kV at room temperature, in marked contrast to thermal ageing for the same time at the effective temperature.

The effect of enhanced diffusion on dislocations and loops clearly depends on the relative absorption rates of interstitials and vacancies. If these rates are equal then the net effect is zero. Preliminary experiments at 600 kV indicate that the interstitial loops in neutron irradiated and annealed copper foils grow during observation at room temperature. In addition to macroscopic climb due to preferential absorption of point defects the dislocations are expected to contain a higher than normal density of jogs because of irradiation. These may be expected to increase the local critical stress for movement, and this must be considered in straining experiments. A more complete account of displacement damage and its effects in the high voltage microscope will be published later.

7. X-ray Production at High Voltages

Penetrating X-rays (Bremstrahlung) are produced when an electron beam is decelerated. X-rays of all energies up to the incident electron energy are produced and the curve of X-ray intensity versus energy peaks at $\sim\frac{1}{2}$ of the beam energy. Although only a small fraction of the energy loss at voltages below 1 MeV is by X-ray production, the photons produced are very penetrating and careful attention must be paid to shielding the operator. The X-ray intensity is approximately proportional to Z for light elements and Z^2 for heavy elements and this can be used to advantage by stopping the beam in aluminium wherever possible. Sufficient shielding at specimen level is required, however, for stopping the beam in a thick area of a heavy element.

High voltage microscopes are shielded only for the normal operating current, and the practice of removing the condenser aperture to pulse heat a specimen will result in a high radiation level outside the column.

8. Application of High Voltage Microscopy

It is useful to consider the areas of work which could benefit most from use of a 1 MV, as opposed to a 100 kV, microscope. The principal advantages are (i) an increase in specimen thickness by a factor of between 3 and 6; (ii) a more rigid specimen [rigidity is proportional to (thickness)^3]; (iii) a reduced ionisation damage rate ($\sim$50%); (iv) much easier dark field facilities; (v) diffraction patterns from small inclusions and precipitates; (vi) increased space for complicated stage experiments; (vii) less sensitivity to external magnetic fields due to increased electron momentum.

The increased penetration (i) will clearly dominate by making serious microscopy possible for the first time on a considerable number of materials which cannot at present be prepared sufficiently thin for 100 kV microscopy. These include materials containing large second-phase particles, large defects such as intergranular voids, some dislocation structures, etc and materials in which the preparation of a thin foil results in changes in the structure to be examined (i.e. dislocation structures in some deformed materials).

In addition, however, and probably even more important, the increased foil thickness will make it possible to study bulk material behaviour directly in the microscope. In many phenomena there is a critical foil thickness below which the behaviour is not typical of bulk material. The critical thicknesses found by Fujita *et al* [13] for various metallurgical processes are given in table VII. It can be seen that in general the thicknesses required are too great for 100 kV

microscopy but are well within the scope of a 1 MV microscope. It is expected therefore that there will be great interest in "in microscope" studies of many metallurgical processes, such as deformation, recrystallisation, phase changes, recovery, etc. In addition the greater penetration will enable specimens to be examined in controlled environments so that processes such as oxidation can be studied as they occur. The encapsulation technique has been used by Dupouy *et al* [25] in an attempt to examine live bacteria and cells.

TABLE VII Critical foil thickness for observation of bulk behaviour (from Fujita *et al* [13]).

Process	Thickness (μm)
Recrystallisation	> 1 (Al, Fe/3% Si)
Martensitic tranformation	> 1 (Cu/11.9% Al)
Dynamic behaviour of dislocations	
(a) Cell formation	> 1.5 (Al)
(b) Three dimensional cell structure	> 3 (Al)
Measurement of dislocation density	> 0.8 (Al)
	> 0.1 (Fe, 5 ppm C)

The reduction in ionisation rate (ii) is clearly attractive to those interested in materials which degrade at 100 kV, such as ionic solids, polymers and biological materials in general. Coupled with image intensification techniques the use of a high voltage microscope presents the best possible advantage for such studies.

(iv) and (v) will attract work from a wide range of investigations primarily being carried out at 100 kV. Many instances arise where knowledge of the structure and nature of small inclusions or precipitates is required. Similarly (iv) will enable the Burgers vectors of a network of dislocations to be analysed very rapidly.

Acknowledgements

The authors are grateful to Dr V. E. Cosslett and the operating staff of the 750 kV electron microscope at the Cavendish Laboratory, Cambridge, for enabling the authors to carry out experiments prior to the installation of the AEI 1 MV microscope at the Atomic Energy Research Establishment, Harwell.

References

1. H. HASHIMOTO, A. HOWIE, and M. J. WHELAN, *Proc. Roy. Soc. A.* **269** (1962) 80.
2. H. YOSHIOKA, *J. Phys. Soc. Japan* **12** (1957) 618.
3. A. HOWIE, *Phil. Mag.* **14** (1966) 223.
4. C. J. HUMPHREYS, Conference on Electron Diffraction, Imperial College, London (1967).
5. V. E. COSSLETT, *J. Roy. Microscop. Soc.* **81** (1962) 1.
6. G. DUPOUY, F. PERRIER, R. UYEDA, R. AYROLES, and A. BOUSQUET, *Compt. rend.* **257** (1963) 1511.
7. L. LANDAU, *J. Phys. (USSR)* **8** (1944) 201.
8. Y. KAMIYA, Proc. Sixth Int. Congr. for Electron Microscopy (Kyoto) I (1966) 95 (Maruzen, Tokyo).
9. V. E. COSSLETT, *Optik* **25** (1967) 383.
10. Y. KAMIYA and R. UYEDA, *J. Phys. Soc. Japan* **16** (1961) 1361.
11. H. HASHIMOTO, K. TANAKA, K. KOBAYASHI, E. SUITO, S. SHIMADZU, and M. IWANAGA, *ibid, Suppl. BII* **17** (1962) 170.
12. G. DUPOUY, F. PERRIER, R. UYEDA, R. AYROLES, and A. MAZEL, *J. Microscop.* **4** (1965) 429.
13. H. FUJITA, Y. KAWASAKI, E. FURUBAYASHI, S. KAJIWARA, and T. TAOKA, *Jap. J. Appl. Phys.* **6** (1967) 214.
14. M. J. GORINGE, A. HOWIE, and M. J. WHELAN, *Phil. Mag.* **14** (1966) 217.
15. R. UYEDA and M. NONOYAMA, *Jap. J. Appl. Phys.* **6** (1967) 557.
16. K. F. HALE, NPL Report FV 10 (1966).
17. J. V. SHARP and D. M. POOLE, unpublished work.
18. G. DUPOUY and F. PERRIER, *Compt. rend.* **258** (1964) 4213.
19. H. A. BETHE, "Handbuch der Physik" (Springer, Berlin) **24** (1933) 273.
20. G. F. BAHR, E. H. ZEITLER, and K. KOBAYASHI, *J. Appl. Phys.* **37** (1966) 2900.
21. R. A. DUGDALE and A. GREEN, *Phil. Mag.* **45** (1954) 163.
22. R. SIGMUND, G. P. SCHEIDLER, and G. ROTH, reported at conference on "Solid State Research with Accelerators" (Brookhaven, USA, 1967).
23. W. M. LOMER, AERE Report T/R 1540 (1954).
24. G. J. DIENES and A. C. DAMASK, *J. Appl. Phys.* **29** (1958) 1713.
25. G. DUPOUY, F. PERRIER, and L. DURRIEU, *Compt. rend.* **251** (1960) 2836.